Impact of Design Methodologies on the Coupler Design and Optimization of an Inductive Power Transfer System

Sampath Jayalath
Department of Electrical Engineering
University of Cape Town
Cape Town, South Africa
sampath.jayalath@uct.ac.za

Azeem Khan
Department of Electrical Engineering
University of Cape Town
Cape Town, South Africa
azeem.khan@uct.ac.za

***Abstract*— Different coil structures such as circular, double D(DD), quadrature DD, bipolar, tripolar, etc., are proposed for inductive power transfer applications. Multi-objective optimization strategies are utilized to optimize these couplers to achieve objectives such as higher efficiency, lower leakage magnetic field, higher power density, lower cost, lower weight, etc. The parameters such as transmitter (Tx)-side inductance, receiver (Rx)-side inductances, and coupling coefficient (k) are constrained depending on the methodology used to design the parameters of the power electronics (PE) system. These PE system parameters are usually the voltage transfer ratio, power rating, total harmonics distortion of the transmitter and receiver current, and external quality factor. Therefore, this paper compares two design methodologies utilized to design and optimize circular couplers of a 3.7 kW IPT system. It identifies critical design equations, similarities, and differences between the two methods, and shows how some design criteria can be used to improve the IPT design process further.**

Keywords*— *Coil design, electric vehicles, inductive power transfer, multi-objective optimization, robust optimization, wireless power transfer

I. Introduction

Inductive power transfer (IPT) technology is at the forefront of realizing fully automated electric vehicles. Therefore, it is critical to improve the performance of the IPT systems to compete in the commercial environment. A typical IPT system consists of input side and output side power electronics and a magnetic coupler. Various power electronics subsystems such as power factor correction converters, high-frequency inverters, filters, impedance matching networks, rectifiers, and impedance converters and coupler structures such as circular, double D(DD), quadrature DD, bipolar, tripolar, etc., are proposed to improve the performance of the IPT system [1].

The couplers are optimized to achieve higher efficiency, lower leakage magnetic field, higher power density, and lower cost and weight [1]. Multi-objective optimization strategies are proposed to optimize the coupler when there is more than one objective to optimize, and Pareto-front of optimal designs are derived [1].

The relationship between the parameters of the power electronics (PE) system and coupler parameters is critical for improving the overall performance of the IPT system [2]. The coupler parameters such as transmitter (Tx)-side inductance (L_{Tx}), receiver (Rx)-side inductance (L_{Rx}) and coupling coefficient (k) are constrained based on the PE system design methodology applied. These constraints are necessary to achieve PE design objectives such as specific voltage transfer ratio, minimum harmonic distortion in the transmitter and receiver current, and avoid frequency bifurcation phenomenon. However, the number of viable optimized solutions resulting from an optimization problem that considers these constraints imposed by PE system design is less compared to optimization problems that do not consider these limitations [1].

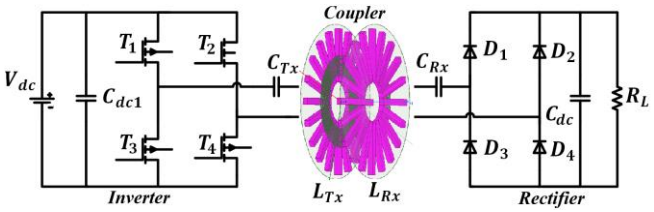

Fig. 1. Circuit diagram of the IPT system.

In this paper, two PE design methodologies are used to optimize circular couplers of two 3.7 kW IPT systems, where constraints are imposed on the coil's parameters such as L_{Tx}, L_{Rx}, and k based on the PE system design objectives discussed above. These two PE design methods are selected for comparison as they use series-series compensation topology and are frequently used for EV applications. In both designs, constraints on coupler parameters are transferred into the finite element analysis (FEA) domain (ANSYS *Maxwell* software) to ensure that constraints are met during optimization. The optimization objectives of both designs are to maximize transmission efficiency (TE) and minimize leakage magnetic field (LMF). Both designs are validated using a 3.7 kW hardware prototype, and a comparison is provided to identify the key features of both designs and their impact on the optimization and performance of the IPT system.

This paper is organized as follows. **Section II** provides the details of the two design methodologies, while **Section III** provides the experimental results and the discussion based on results. **Section IV** concludes the paper.

II. System Design

This paper considers two PE design methodologies for a 3.7 kW series-series compensated IPT system. Circular couplers with an air gap of 150 mm are optimized using both methods. The input and output voltages of the IPT system are designed to be less than 350 V. **Fig. 1** shows the circuit diagram of the IPT system, where the operating frequency of the inverter is 85 kHz. The series-series (SS) compensation is utilized by

TABLE I
DESIGN OBJECTIVES AND EQUATIONS OF DESIGN ONE AND TWO

	Objectives	***Equations***	
		Design One	***Design Two***
1	Minimize the harmonics of I_{Rx} due to the non-linearity of class D rectifiers.	$\frac{\omega_0 L_{Rx}}{R_L} \approx \frac{8Q_e}{\pi^2} \geq 3$ (1)	*NA*
2	Avoid frequency bifurcation phenomenon in input impedance. Minimize the harmonics of I_{Tx} due to the non-linearity in the resonant inverter.	$k_0 < k_c \approx \frac{1}{Q_e}$ (2) $k_0 \leq k_s \approx \frac{1}{\sqrt{2}Q_e}$ (3) $\left(L_{Rx} \approx \frac{R_e}{\sqrt{2}\omega_0 k_0}\right) \geq \left(\frac{3\pi^2 R_e}{8\omega_0}\right)$ (4) $k_0 \leq k_{0m} = \frac{8}{3\pi^2}\sqrt{\frac{1}{2}}$ (5)	$K_{p(max)}\left(\frac{R_e}{\omega_0 k}\right) < L_{Rx} < K_{p(\min)}\left(\frac{R_e}{\omega_0 k}\right)$ (7) $k_0 < k_c \approx \frac{1}{Q_e}$ (8)
3	To achieve the desired voltage transfer ratio.	$V_{TR}(\omega_0) \approx \sqrt{2}\sqrt{L_{Rx}/L_{Tx}}$ (6)	$L_{Tx} \approx \left(\frac{R_e}{\omega_0 k}\right)(G_v(\omega_0))^2$ (9)

I_{Rx}- Rx-side current, I_{Tx}- Tx-side current, ω_0-radian operating frequency, R_L-load resistance as shown in **Fig. 1**, Q_e- external quality factor ($=\omega_0 L_{Rx}/R_e$), $R_e=(8R_L)/\pi^2$, *kc*-critical coupling coefficient, *ks*- split coupling coefficient, k_{om}- maximum value of nominal coupling coefficient, $K_{p(max)}$ a factor that varies in the range of 0.65-0.85.

both designs[1]. The output is modeled as a resistor (R_L). The high-frequency *ac* output is rectified with a class D rectifier and provided to load R_L.

A. Design Methodologies

Table I provides the design equations used by both methodologies to achieve specific objectives. These objectives are related to the operation of the PE system of the IPT system [4],[5]. Parameter definitions are provided in the footnote of **Table I**. In both designs, the coupler parameters impacted or limited by the PE system design are the L_{Tx}, L_{Rx}, and *k*.

In design one, equations (1)-(5) must be satisfied to meet the stated objectives *one* and *two* [4]. However, the parameter Q_e is common to both (1), (2) and (3). The value of L_{Rx} to meet the design criteria stated in equation (1), (2) and (3) are given by (4). Therefore, equation (4) is used to design the value of L_{Rx} to meet the objectives of lower harmonics in I_{Tx} and I_{Rx}. Furthermore, the coupling coefficient is designed according to equation (5), to satisfy the inequality given by (4). The parameter L_{Tx} is designed to achieve the desired voltage transfer ratio (VTR) according to equation (6).

Design two does not incorporate objective one into its methodology, but L_{Rx} is designed according to (7) to ensure objective two [5]. The factor $K_{p(max)}$ is introduced in this paper and varies in the range of 0.65-0.85 to ensure the design meets (8). This range will have limited impact in ensuring maximum TE as its maxima are relatively constant [5]. The parameter L_{Tx} is designed to achieve the desired VTR at optimally matched load conditions[3][5]. The coupling coefficient is limited by (8) in design two, which is also the same requirement for design one according to (2).

It is evident that the coupler parameters such as L_{Tx}, L_{Rx} and *k* must be designed appropriately to achieve the objectives listed in **Table I**. Therefore, the limits on these parameters must be conformed during the optimization.

B. Multi-objective optimization

The circular couplers of the two designs are optimized to achieve higher power *TE* and lower *LMF* at the perfectly aligned position with an air gap of 150 mm. *TE* can be maximized by improving the *k* and coil's quality factors [3]. However, increase in *k* tends to increase the *LMF* measured at a point which needs to be minimized. Therefore, Pareto-fronts for both designs are derived as the objectives have conflicting characteristics [1]. Both designs are optimized by

TABLE II
OPTIMIZATION CONSTRAINTS OF DESIGN ONE AND TWO

Parameter	**Design One**	**Design Two**
L_{Rx}	*Equation (4)*	*Equation (7)*
L_{Tx}	*Equation (6)*	*Equation (9)*
k_o	*Equation (2),(3),(5)*	*Equation (8)*
$B_{s(min)}$ *at 650mm*	<27 μT	
η_{coil}	> 95%	
A_c	< 0.30 m^2	
h	150 mm	
f	85 kHz	
B_{Fe}	< 200 mT	

TABLE III
DESIGN VARIABLES OF DESIGN ONE AND TWO

Design Variable	Design One	Design Two
r_{iT}/r_i	102.24	113/100
r_{wT}/r_w	1.907	1.98/2.10
r_{cT}/r_c	0.59	0.6/1.5
r_{sT}/r_s	298.2	297/300.2
h_{wfT}/h_{wf}	1.45	3.74/3.74
h_{fsT}/h_{fs}	2.5	2.5/2.5
t_{sT}/t_s	0.75	2/2.02
r_{fT}/r_f	80.5	80.4/81
N_T/N_R	17	18/14
t_{fT}/t_f	25	25/25
w_{fT}/w_f	25	25/25
l_{fT}/l_f	202	202/202

TABLE IV
OPTIMIZATION AND EXPERIMENTAL RESULTS OF DESIGN ONE AND TWO

Par	**Design One**		**Design Two**	
	Sim	Fab	Sim	Fab
L_{Tx}	207.51μH	188.06μH	228.40 μH	236.98μH
L_{Rx}	207.60μH	188.70μH	127.69 μH	130.82μH
k	0.164	0.1765	0.220	0.2276
TE	97.5%	96.5%	96.96 %	96.90 %
LMF (650mm)	6.73 μT	7.40 μT	7.01 μT	7.78 μT
$VTR(V_{Rx}/V_{Tx})$	$\sqrt{2}$	1.5	0.8571	0.8563
THD (I_{Tx})	2.33%	2.45%	2.62%	2.24%
THD (I_{Rx})	3.00%	3.42%	3.90%	3.85%

Par- Parameters, Sim- Simulated/Optimized design, Fab- Fabricated design.

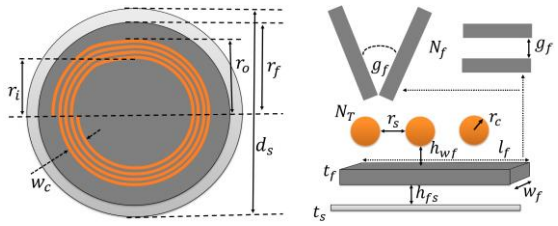

Fig. 2. Design variables of the circular coil [1].

considering similar coupler constraints except for the constraints imposed by the PE system design. All the limitations are listed under **Table II**. The design variables of a circular coil are shown in **Fig. 2**. It consists of a copper winding, ferrite sheet or blocks, and a passive shield. The design variables used in this comparison are listed in **Table III**. The design variables of the Tx and Rx-coils of design one are identical while they are different for design two. Design variables with subscript *T* correspond to the Tx-coil.

Sensitivity analysis was used to identify the critical design variables of both designs to reduce the computation time by ignoring less important design variables from optimization [1]. In design one, h_{wf}, h_{wfT}, and t_s are excluded from the optimization, while h_{wf}, h_{wfT}, h_{fs}, and h_{fsT} are the design variables excluded in design two based on the results of the sensitivity analysis. These design variables are kept at their initial values during the optimization.

In literature, the theoretical and practical values of the parameters such as L_{Tx}, L_{Rx}, and k vary significantly due to the manufacturing and fabrication tolerances of the coil design variables [4]. In an IPT coupler, manufacturing tolerances are slight variations in dimensions of the core and passive shielding materials and the diameter of Litz wire from the expected/mean values due to the imperfections in the manufacturing process. The fabrication tolerances arise due to difficulties in realizing the exact value of the optimized design variable. For example, the design variables such as space between the turns (r_c) are challenging to realize and can significantly impact the parameters such as the coupling coefficient [6]. In this paper, both designs considered the impact of manufacturing and fabrication tolerances during the optimization by incorporating the concept of robust optimization. Therefore, both designs ensured that limitations imposed on the coupler parameters such as L_{Tx}, L_{Rx}, and k based on the design of the PE system as given by (1)-(8), are not violated by the fabricated coupler due to the manufacturing and fabrication tolerances. Design two considered the impact of misalignment when selecting the best design for implementation from the Pareto front of the optimal designs (*six valid designs*) shown in **Fig. 3**. However, the design variables of both designs (*one* and *two*) are optimized for a perfectly aligned coupler with an air gap of 150 mm. The optimized values of design variables are listed in **Table III.** Many optimized solutions were not Pareto optimal or violated the constraints imposed by inequalities (1)-(8). These solutions were ignored when deriving the Pareto-front of optimal designs and not shown in **Fig. 3**. An evolutionary algorithm (EA) is used to derive the Pareto-front of the optimized coil designs due to its superiority in handling multiple constraints and objectives. The designs on the Pareto-front of both methods achieve similar values for objectives, as seen from **Fig. 3**. Therefore, it is reasonable to

TABLE V
CONSTRAINTS COMPARISON BETWEEN DESIGN ONE AND TWO

Par	Design One				Design two			
	Sim	C	Fab	C	Sim	C	Fab	C
$k< k_c$	0.164< 0.242	Y	0.176< 0.2663	Y	0.216< 0.289	Y	0.227< 0.282	Y
$8Q_e/\pi^2 \geq 3$	3.35	Y	3.04	Y	2.80	*N*	2.87	*N*

Sim- Simulated/Optimized design, Fab- Fabricated design, C-Does the design meet the criteria, Y-Yes, N-No.

compare the results of the two designs at the perfectly aligned positions to identify the impact of PE system design methodologies on the optimization and performance of the IPT system.

III. EXPERIMENTAL RESULTS AND DISCUSSION

Designs ***A*** and ***B*** are selected for implementation from the Pareto-front of optimal designs shown in **Fig. 3**. The optimized and fabricated coupler's parameters and results are shown in **Table IV**. There is a relatively large variation between the optimized (simulated) and fabricated coupler parameters such as k, L_{Tx}, and L_{Rx} of design one compared to design two. It is mainly due to the introduction of slightly higher manufacturing and fabrication tolerances with the fabricated coupler of design one to show the robustness of the optimized solution in the presence of manufacturing and fabrication tolerances. The design's L_{Rx} needs to be greater than 186 µH according to (4) to satisfy design objective *two*. In this study, it is not violated by the fabricated coupler even at the expense of manufacturing and fabrication tolerances in design variables. The L_{Tx} and L_{Rx} are equal in design one as VTR of $\sqrt{2}$ is used for the IPT system, while L_{Rx} is small compared to L_{Tx} in design two to satisfy design objective *two*.

Fig. 4 shows the experimental setup of the IPT system. **Fig. 5** shows Tx-side and Rx-side currents and voltages of both designs, and the TE, LMF, VTR, and total harmonics

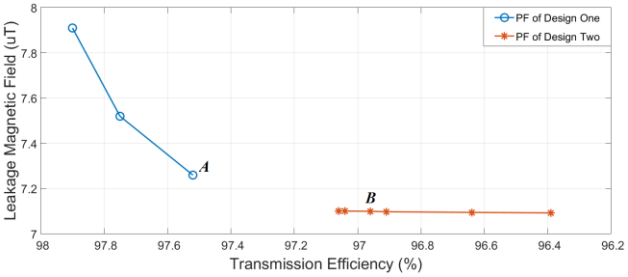

Fig. 3. Pareto-fronts of the optimized designs.

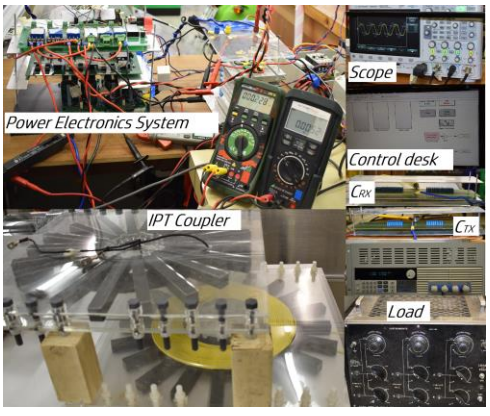

Fig. 4. Experimental setup of the IPT system.

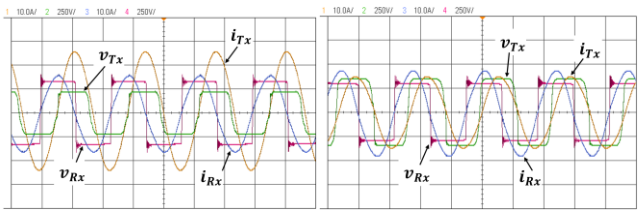

(a) (b)

Fig. 5. Transmitter-side and receiver-side current and voltage waveforms (a). Design one, (b). Design two.

distortion (THD) of the I_{Tx} and I_{Rx} are listed in **Table IV**. There is hardly any difference in the efficiencies and the leakage magnetic fields of both designs. The leakage magnetic field is evaluated at 650 mm from the center of the coil and both designs comply with the 27μT upper limit of leakage magnetic field defined in SAE J2954/1 STD. Therefore, the impact of both design methodologies on the performance of the coupler is minimal.

The transmitter-side voltage is higher in design two than in design one due to the lower VTR. This is because the input and output voltages are limited to less than 350V in this study. Furthermore, there is a slight variation in simulated and measured VTR due to discrepancies between the simulated and fabricated coupler parameters.

The THD can be used to evaluate the harmonic mitigation of both designs. The THD of I_{Tx} of both designs is well below 5%. Both designs comply with (2) and (8), as shown in **Table V**, which is a criterion to reduce the harmonic distortion of the transmitter current due to the non-linearity in the resonant inverter and to avoid the frequency bifurcation phenomena in the input impedance. Both designs have a zero-phase angle frequency in the input impedance as shown in **Fig. 6**. Therefore, the frequency bifurcation phenomenon is avoided. The magnitudes of the input impedances of both implemented systems are plotted as a function of frequency as shown in **Fig. 7**, to understand the harmonic attenuation of I_{Tx} of both designs. It is evident that in design two's harmonics with respect to operating frequency see a higher impedance compared to design one and justify the reason for the slight reduction in THD of I_{Tx} in design two compared to one. The Z_{in} and Arg (Z_{in}) are a function of coil parameters. These parameters are different for both optimized designs, as shown in **Table IV**. As a result, discrepancies are seen in **Fig. 6** and **Fig. 7** for both designs.

The THD of I_{Rx} is also below 5%. However, the design two has a slightly higher THD compared to one. Equation (1) is a design requirement for design one and not for design two to reduce the harmonics of I_{Rx}. Therefore, inequality (1) is marginally violated by design two, as shown in Table **V**. Theoretically, an $L_{Rx} > 136.63$ μH can satisfy the inequality (1) for design two. In this study, none of the Pareto optimal solutions of design two shown in **Fig. 3** did not satisfy this condition, while all the Pareto optimal solutions of design one satisfied this condition, as it was incorporated into the design methodology. However, the primary purpose of (1) is to minimize the harmonics of I_{Rx} and not to restrict it to a specific limit [7]. Therefore, further studies are encouraged to determine the relationships and impact of limiting the harmonics to specific limits on the parameters of the coupler, the optimization process, and the performance of the IPT system. Nevertheless, inequality (1) can be incorporated into design two if required, as discussed above.

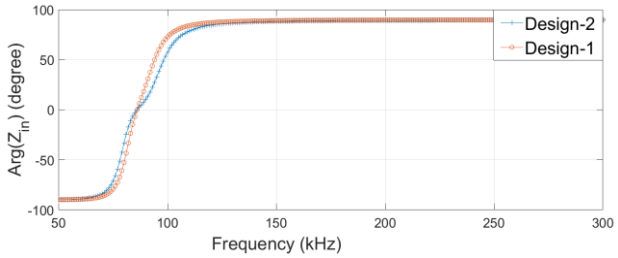

Fig. 6. The phase angle of input impedance of designs one and two as a function of frequency.

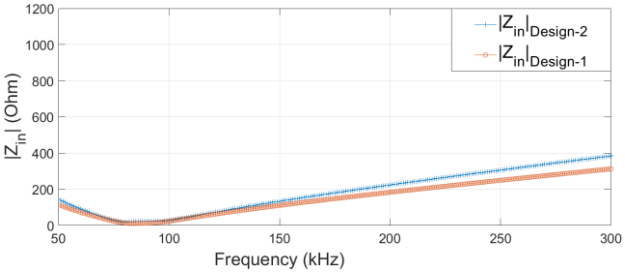

Fig. 7. The input impedances of designs one and two as a function of frequency.

IV. Conclusion

This paper compares two power electronics design methodologies to identify their impact on the coupler optimization and performance of the IPT system. The design objectives and corresponding design equations are provided, which can be used with any IPT application. The coil parameters such as transmitter side inductance, receiver side inductance, coupling coefficient vary considerably due to the approach used by the two methods to achieve design objectives. However, the optimized couplers resulting from both designs can achieve similar higher transmission efficiencies and lower leakage magnetic fields. The harmonics in the transmitter and receiver current are minimal in both designs with minor variations. The design's coupling coefficient value compared to the critical coupling coefficient dictates the attenuation of harmonics in the transmitter current, while the loaded quality factor value determines the attenuation of the harmonics in the receiver current.

Acknowledgment

The authors acknowledge Naomi Harrisankar, Maysam Soltanian, Riyaad Jacobs, and Hoosain Salie for their assistance with the experimental setup.

References

[1] S. Jayalath and A. Khan, "Design, Challenges, and Trends of Inductive Power Transfer Couplers for Electric Vehicles: A Review," *IEEE J. Emerg. Sel. Topics Power Electron*., vol. 9, no. 5, pp. 6196-6218, Oct. 2021.

[2] S. Jayalath and A. Khan, “Analysis of the Relationship between the Parameters of IPT Transformer and Power Electronic System,” *Proc. IEEE Wireless Power Transf. Conf. (WPTC)*, Qubec, Canada, 2017, pp. 1-4.

[3] R. Bosshard, J. W. Kolar, J. Mühlethaler, I. Stevanović, B. Wunsch, F. Canales, " Modeling and \$eta \$ - \$alpha \$ -Pareto optimization of inductive power transfer coils for electric vehicles ", *IEEE J. Emerg. Sel. Topics Power Electron*., vol. 3, no. 1, pp. 50-64, Mar. 2015.

[4] H. Kim et al., "Coil Design and Measurements of Automotive Magnetic Resonant Wireless Charging System for High-Efficiency and Low Magnetic Field Leakage," *IEEE Trans.Microw. Theory Techn.*, vol. 64, no. 2, pp. 383-400, Feb. 2016.

[5] R. Bosshard, Multi-Objective Optimization of Inductive Power Transfer Systems for EV Charging. Zürich, Switzerland: ETH Zurich, 2015.

[6] A. A. S. Mohamed, S. An and O. Mohammed, "Coil Design Optimization of Power Pad in IPT System for Electric Vehicle Applications," *IEEE Trans. Magn.*, vol. 54, no. 4, pp. 1-5, April 2018.

[7] M. K. Kazimierczuk and D. Czarkowski, Resonant Power Converters, 2nd ed. New York, NY, USA: Wiley, 2011.